INTERNATIONAL JOURNAL FOR NUMERICAL METHODS IN FLUIDS, VOL. 13, 857–867 (1991)

THREE-DIMENSIONAL SIMULATIONS OF NATURAL CONVECTION IN A SIDEWALL-HEATED CUBE

TORU FUSEGI

Institute of Computational Fluids Dynamics, 1-22-3 Haramachi, Meguro, Tokyo 152, Japan

JAE MIN HYUN

Department of Mechanical Engineering, Korea Advanced Institute of Science and Technology, Chong Ryang, Seoul 131, Korea

AND

KUNIO KUWAHARA

Institute of Space and Astronautical Science, 3-1-1 Yoshinodai, Sagamihara, Kanagawa 229, Japan

SUMMARY

A high-resolution, finite difference numerical study is reported on three-dimensional natural convection of air in a differentially heated cubical enclosure over an extensive range of Rayleigh number from 10^3 to 10^{10}. The maximum number of grid points is $122 \times 62 \times 62$. Solutions to the primitive variable formulation of the incompressible Navier–Stokes and energy equations are acquired by a control-volume-based procedure together with a higher-order upwind-differencing technique. The field characteristics at large-time limits are examined in detail by state-of-the-art numerical visualizations of the three-dimensional results. The emergence of the well-defined boundary layers and the interior core at high Rayleigh numbers is captured by elaborate numerical visualizations. Both the similarities and discrepancies between the three- and two-dimensional computations are pointed out. These emphasize the need for three-dimensional calculations to accurately determine the flow characteristics and heat transfer properties in realistic, high-Rayleigh-number situations.

KEY WORDS Natural convection Finite difference method Direct numerical simulations Three-dimensional graphics

INTRODUCTION

Natural convection flows in enclosures arise in a variety of thermal engineering systems. Applications are found in solar energy collectors and storage devices, electronic equipment cooling, ventilation of buildings and compartment fires, to cite a few. Research efforts in these fields were concentrated on laboratory experiments and numerical simulations. With the advent of high-speed computers, numerical computations of such complex fluid phenomena have gained momentum of late.

The majority of the preceding numerical studies have been two-dimensional. This was unavoidable in view of the limited capability of the computing resources as well as the prohibitively high cost of computations. Various numerical schemes were explored and tested. Owing to these strenuous endeavours, a considerable body of knowledge has been accumulated

0271–2091/91/170857–11$05.50

Received September 1990
Revised December 1990

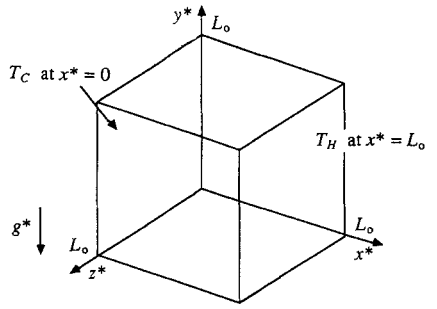

Figure 1. The geometry and boundary conditions of the problem. The walls are thermally insulated unless otherwise noted

on the principal characteristics of two-dimensional convective flows in geometrically simple enclosures. In the present paper a cubical enclosure is considered. This represents a well-documented configuration. The major attractiveness is that the boundary conditions are straightforward; consequently, the pertinent physics can be studied in depth, without being distracted by other complicated features.

The specific flow under consideration is the natural convection of air in a cubical enclosure, of which two vertical sidewalls ($x^* = 0$ and L_0) are differentially heated. As sketched in Figure 1, the temperatures of the sidewalls are T_C (at $x^* = 0$) and T_H (at $x^* = L_0$), where $T_H > T_C$. These 'heating-by-the-side' convective flows have been widely investigated.[1]

The two-dimensional numerical computations of this flow have been carried out over a broad range of Rayleigh number, $10^3 \leqslant Ra \leqslant 10^{16}$. Markatos and Pericleous[2] assumed laminar flows up to $Ra = 10^6$. For higher Rayleigh numbers the k–ε turbulence model was invoked. A set of benchmark numerical solutions[3] has been suggested in the range $10^3 \leqslant Ra \leqslant 10^6$ for a Boussinesq fluid of $Pr = 0{\cdot}71$. Mention is made of these representative works to underscore the breadth and scope of the past numerical examinations.

As to the numerical calculations of very high-Rayleigh-number flows, a direct numerical simulation technique was employed for a two-dimensional cavity.[4] Some of the prominent features were disclosed and qualitative comparisons with the experiments were attempted.

Another important research field of concern is the transient behaviour of convective flows in the cavity when the differential heating is applied abruptly to the system. Patterson and Imberger,[5] by way of a physically plausible scaling argument, proposed classifications of the types of transient flows. Experimental verifications of the main contentions of the scaling analysis were reported in the literature.[6] The transient convection in a cavity has also been the subject of intense numerical computations. The prior two-dimensional numerical simulations[4, 7, 8] revealed qualitative consistency with some of the analytical predictions.[5]

It is needless to state that, in order to move closer to practical systems, three-dimensional flow and heat transfer calculations are highly desirable. However, owing to the obvious reason of the restricted availability of computational resources, full-scale three-dimensional simulations have been in an infant stage. Several three-dimensional numerical solutions have been illustrated[9–11] which demonstrated three-dimensional flow structures in a rectangular box. However, the previous three-dimensional computations have suffered mostly from the lack of proper resolution. Relatively coarse finite difference meshes (the largest number of grid points used was $45 \times 45 \times 20$)[11] were employed in these preceding calculations. Another crucial area that needs

significant improvement is numerical visualization techniques. Since the field is three-dimensional in nature, proper and accurate interpretations of the numerical results may be greatly aided only by use of the elaborate three-dimensional computer graphics capabilities.

This paper describes a comprehensive series of recent efforts to delineate the three-dimensional natural convection in a cubical box. The unapproximated three-dimensional Navier–Stokes and energy equations are solved numerically on an extremely fine mesh. The accessibility to a high-power supercomputer system made it possible to embark on such extensive numerical computations. The purpose here is to portray the computational procedure of three-dimensional cavity flows driven by the differential heating of the vertical sidewalls.

In this paper, exemplary results of such three-dimensional calculations of large-time behaviour as well as transient processes of the convective flows are illuminated. Of particular relevance is the implementation of state-of-the-art numerical visualization techniques to the three-dimensional results. These exercises will set the stage for further systematically organized numerical simulations of more complex flow geometries.

MATHEMATICAL MODEL

The flow is governed by the incompressible unsteady Navier–Stokes and energy equations. The Boussinesq approximation is invoked for the fluid property variation. The non-dimensionalized form of the basic equations can be expressed in tensor notation as

$$\frac{\partial u_j}{\partial x_j}=0, \tag{1}$$

$$\frac{\partial u_i}{\partial t}+\frac{\partial}{\partial x_j}(u_j u_i)=-\frac{\partial p}{\partial x_i}+\frac{1}{Re}\frac{\partial^2 u_i}{\partial x_j \partial x_j}+\delta_{i2}\frac{T-1}{Fr}, \tag{2}$$

$$\frac{\partial T}{\partial t}+\frac{\partial}{\partial x_j}(u_j T)=\frac{1}{Re\,Pr}\frac{\partial^2 T}{\partial x_j \partial x_j}, \tag{3}$$

where δ_{ij} is the Kronecker delta ($\delta_{ij}=1$ if $i=j$; $\delta_{ij}=0$ otherwise). The viscous dissipation and the pressure work terms are neglected in the energy equation.

The physical quantities are non-dimensionalized in the following manner.

$$(x, y, z)=(x^*, y^*, z^*)/L_0, \qquad (u, v, w)=(u^*, v^*, w^*)/u_0,$$
$$t=t^* u_0/L_0, \qquad p=(p^*-p_0)/\rho^* u_0^2, \qquad T=T^*/T_0,$$

where asterisks denote dimensional values. The reference scales for length, velocity, time, pressure and temperature are the enclosure height (L_0), the convective velocity ($u_0=[g^*\beta^* L_0(T_H-T_C)]^{1/2}$), the convective time ($t_0=[g^*\beta^*(T_H-T_C)/L_0]^{-1/2}=N^{-1}$, where N is the Brunt–Väisälä frequency), the hydrostatic pressure (p_0) and the film temperature ($T_0=(T_C+T_H)/2$) respectively. In the present form of non-dimensionalization the Reynolds, Prandtl and Rayleigh numbers are related by $Ra=Re^2 Pr$.

In accordance with the problem statement the boundary conditions are

$$u=v=w=0 \quad \text{on all the walls,} \tag{4}$$

$$T=(2-\delta)/2 \quad \text{at } x=0, \quad T=(2+\delta)/2 \quad \text{at } x=1, \quad \partial T/\partial n=0 \quad \text{at } y=0, 1 \text{ and } z=0, 1, \tag{5}$$

where n denotes the co-ordinate normal to the surface. The overheat ratio δ is set at 0·1 in the present study. The Prandtl number Pr is equal to 0·71.

Table I. The parameters of the computations

	Finite difference mesh			
Ra	No. of grid points	Minimum spacing*	Spacing ratio†	Time increment*
10^3	$32\times32\times32$	$3{\cdot}33\times10^{-2}$	1	—
10^4	$62\times62\times62$	$1{\cdot}67\times10^{-2}$	1	—
10^5	$62\times62\times62$	$1{\cdot}58\times10^{-2}$	2	—
10^6	$62\times62\times62$	$1{\cdot}49\times10^{-2}$	3	1·0
10^8	$62\times62\times62$	$8{\cdot}0\times10^{-3}$	7	0·1
10^{10}	$122\times62\times62$	$1{\cdot}3\times10^{-3}$	20	0·1

* Non-dimensional values.
† Maximum grid spacing/minimum grid spacing.

SOLUTION METHOD

A discretized form of the governing equation system (1)–(5) is obtained through a control-volume-based finite difference procedure. Numerical solutions are acquired by an iterative method together with the pressure correction algorithm SIMPLE.[12] The present technique employs the strongly implicit scheme (SIP)[13] to accelerate the convergence characteristics of the solutions. SIP is applied to the planes of constant z in order to determine simultaneously the dependent variables in the x- and y-directions on each plane.

The convection terms in the momentum equation (2) are treated by the QUICK methodology modified for non-uniform grids,[14] while those in the energy equation (3) are dealt with by a hybrid scheme.[12] The QUICK scheme involves a third-order-accurate upwind differencing, which possesses the stability of the first-order upwind formula and is free from substantial numerical diffusion experienced with the usual first-order techniques. Transient calculations are conducted by an implicit method to march in time.

The entire enclosure constituted the full computational domain. The particulars of the computations are summarized in Table I. Variable grid spacing is introduced to resolve steep gradients of the velocity and the temperature near the walls. The grid dependence of the solutions has been checked at $Ra=10^6$ by a series of test computations in which the grid spacing was varied systematically. Changes in the peak velocity were less than 2% when the number of grid points was doubled in the x-direction. A much smaller variation of 0·2% was observed in the overall Nusselt number at the isothermal sidewalls.

Convergence of computations is declared when the following criterion is met:

$$\frac{|\phi_n-\phi_{n-1}|}{|\phi_n|_{\text{maximum}}}\leqslant10^{-4} \quad \text{for all } \phi, \tag{6}$$

where ϕ denotes any dependent variable and n indicates the value of ϕ at the nth iteration level.

When the steady state flows are of interest, a converged solution at a lower Rayleigh number is used as the initial condition for a new (higher) Rayleigh number. However, at the highest Rayleigh number studied, i.e. $Ra=10^{10}$, the field data of the two-dimensional calculation at the same Rayleigh number were implemented in the three-dimensional computational domain as its initial condition. Time steps are advanced until the effect of the initial condition becomes negligible in the result.

RESULTS AND DISCUSSION

Computations were performed on a Hitachi S-820/80 supercomputer system at the Institute of Computational Fluid Dynamics (ICFD) in Tokyo, Japan. The system has a maximum CPU speed of 3 Gflops and a maximum in-core memory of 512 MB. A typical computation for $Ra \leqslant 10^7$ required a CPU time of 30 min with 600 iterations and 100 MB of the memory. When $Ra > 10^7$, transient calculations were made and consequently the CPU time increased drastically; at $Ra = 10^{10}$ it took nearly 14 h to advance 1600 steps in time.

Steady states were reached when $Ra \leqslant 10^8$. At a higher Rayleigh number, say 10^{10}, the fields did not appear to attain strictly steady states, as described later.

The present section is divided into two parts. The overall field characteristics are examined first by three-dimensional numerical visualizations of the data for the Rayleigh number range at which the steady state was obtained ($Ra \leqslant 10^8$). Then the case with periodic fluctuations ($Ra = 10^{10}$) is considered. The heat transfer rate across the enclosure is presented for the entire range of Rayleigh number studied, i.e., $10^3 \leqslant Ra \leqslant 10^{10}$.

The three-dimensional graphics to be reproduced in this section were generated by an interactive graphic software[15] which runs on a Fujitsu VP-200 supercomputer system at the ICFD.

Steady state characteristics ($10^3 \leqslant Ra \leqslant 10^8$)

As a representative case for natural convection flows at a relatively low Rayleigh number, the isotherm surfaces and the absolute values of the vorticity (the magnitude of the vorticity vector) at $Ra = 10^4$ are depicted in Plate 1. The global isotherm patterns in the bulk of the enclosure are qualitatively similar to those of the two-dimensional flows previously obtained;[3] however, in the z-direction, three-dimensional variations are observed, especially near the endwalls ($z = 0$ and 1). The half-domain in $0{\cdot}5 < z < 1$ is the mirror image of the other half in $0 < z < 0{\cdot}5$ about the plane $z = 0{\cdot}5$. In addition, the cross-sections of the field in the z-direction are centrosymmetric with respect to the centre of the cavity ($x = 0{\cdot}5$, $y = 0{\cdot}5$). The magnitudes of the vorticity are large in the regions close to the isothermal sidewalls. The existence of the unicellular flow can also be inferred by the vorticity plots.

As the Rayleigh number increases, the field is characterized by the boundary layers near the isothermal sidewalls ($x = 0$ and 1) and the near-stagnant interior core structure in the central region, as described in Plate 2. At $Ra = 10^6$ a pair of thin thermal boundary layers is seen along the isothermal walls and the temperature stratification is evident in the interior core. Three-dimensional variations are noticeable near the endwalls ($z = 0$ and 1); however, the temperature field shows relatively weak z-dependences in the interior core. The contours of the absolute vorticity clearly demonstrate the distinct boundary layers and the near-stagnant interior core structure of the flow field. The three-dimensionalities are prominent only near the endwalls, similar to the temperature field discussed earlier. It is noteworthy that regions of weak vortices are found in the areas where the isothermal vertical sidewalls abut the adiabatic endwalls. The presence of these regions extends over the entire height of the enclosure. These secondary vortices have also been documented by the earlier numerical simulations[11] which dealt with an enclosure of aspect ratio $A_z = 2$.

The field data in the midplane ($z = 0{\cdot}5$) are consistent with the two-dimensional solutions[3] in the range $10^3 \leqslant Ra \leqslant 10^6$ as reported elsewhere.[16]

The results for $Ra = 10^8$ (not shown) are qualitatively similar to those for $Ra = 10^6$. Owing to the enhanced convective activity, the boundary layers near the sidewalls are thinner at $Ra = 10^8$ than in the lower-Ra case.

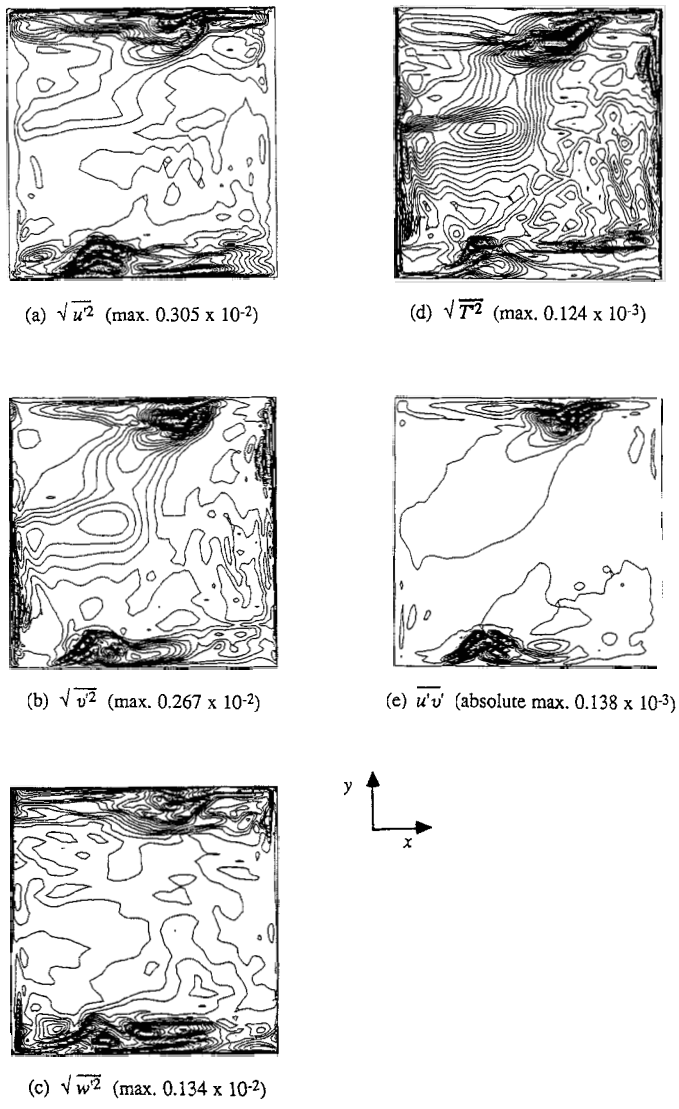

(a) $\sqrt{\overline{u'^2}}$ (max. 0.305 x 10^{-2})

(d) $\sqrt{\overline{T'^2}}$ (max. 0.124 x 10^{-3})

(b) $\sqrt{\overline{v'^2}}$ (max. 0.267 x 10^{-2})

(e) $\overline{u'v'}$ (absolute max. 0.138 x 10^{-3})

(c) $\sqrt{\overline{w'^2}}$ (max. 0.134 x 10^{-2})

Figure 2. Root mean squares and a cross-correlation of the fluctuation components in the mid-plane $z=0{\cdot}5$ at $Ra=10^{10}$

Field characteristics at a higher Rayleigh number ($Ra=10^{10}$)

The time-averaged fields are scrutinized first in this subsection by inspecting the isotherms and the isosurfaces of the absolute values of the vorticity as depicted in Plate 3. The instantaneous fields are averaged over a time interval which is sufficiently large compared to the dominant time scale of the flow. The time-averaged fields can be characterized by well-developed boundary layers along the isothermal sidewalls and a near-stagnant inner core. The thickness of the boundary layers is significantly reduced compared to the previous cases (see Plate 2). Even in the mean fields, appreciable three-dimensional variations of the isotherms and vorticity contour surfaces are evident. These irregularities were smoothed out in the results obtained with the k–ε turbulence model[11] in the case of an enclosure with a depth-to-width ratio of 2·0 at $Ra=10^{10}$.

The root mean squares (RMS) and a cross-correlation of the turbulent fluctuations in the plane located at $z=0{\cdot}5$ are displayed in Figure 2. These quantities are defined as

$$\overline{\phi_i' \phi_j'} = \frac{1}{\Delta t} \int_{t_0}^{t_0+\Delta t} \phi_i' \phi_j' \, \mathrm{d}t, \tag{7}$$

where ϕ_i' denotes the fluctuating component of any variable ϕ_i, t_0 is the reference time level and Δt represents the time interval. High concentrations of the quantities are notable in regions in the vicinity of the walls. In all the fields depicted in Figure 2 these areas appear near the horizontal walls small distances away from the upper-left and lower-right corners. The boundary layers which flow near the isothermal vertical walls turn their directions sharply at the corners and then discharge into the near-stagnant central core (see also Plate 3). Large magnitudes of shear are generated when the fluid discharge takes place. These regions correspond to those of high concentrations of the correlations near the horizontal walls. In the vertical velocity and temperature fluctuations (Figures 2(b) and 2(d)), very thin layers of high concentrations of $\overline{v'^2}$ and $\overline{T'^2}$ are discernible adjacent to the sidewalls. Steep velocity gradients between the boundary layers and the stationary walls and between the boundary layers and the near stagnant central core are attributed to the generation of high shears.

In the present results the cross-correlation of the horizontal and vertical components of velocity seems to be of the same order of magnitude as those of the mean fluctuations. The temperature fluctuations are found to be one order of magnitude smaller than those for the velocity components. Inspection of the results (not shown) reveals that the overall magnitudes of the correlations attain very small values near the endwalls where the velocities are low.

Time histories of the local temperature at $(x, y, z)=(0{\cdot}51, 0{\cdot}81, 0{\cdot}517)$ and the overall Nusselt number (defined by equations (8) and (9)) at the cooled wall ($x=0$) are plotted in Figure 3. Periodic oscillations in the temperature are visible and for the Nusselt number the period appears to be comparable to that of the temperature. Figure 4 displays the Nusselt number in the midplane $z=0{\cdot}5$. The amplitude of the fluctuations decreases as time elapses, which is suggestive of the decay of the internal gravity wave present in the enclosure.[5]

The internal gravity wave in differentially heated two-dimensional enclosures has been extensively investigated for low-Rayleigh-number flows (see e.g. References 5 and 17). Patterson and Imberger[5] attributed the mechanics of the generation and subsequent decay of the internal gravity wave to the initial *piling up* of fluids with different temperatures at the enclosure corners. The piling up of fluid layers creates temperature inversion in these regions. This generates the internal gravity wave, which travels between the isothermal walls across the enclosure. The period of the oscillations for the present results is approximately 8·0, which is in reasonable agreement with the theoretical value for two-dimensional flows[5, 17] of $(2\sqrt{2})\pi$ $(=8{\cdot}89)$. This period also characterizes the oscillatory behaviour of the temperature and the Nusselt number, as pointed out in the previous figure.

Heat transfer results

The non-dimensionalized heat transfer rate at a plane $x=a$ is represented by the Nusselt numbers. These quantities are defined as follows:

$$Nu_{\text{mean}}(z) = \int_0^1 \left(-\frac{\partial T}{\partial x}(x=a, y, z) + Re\, Pr\, u(T(x=a, y, z)-1) \right) \mathrm{d}y, \tag{8}$$

$$Nu_{\text{overall}} = \int_0^1 Nu_{\text{mean}}(z) \, \mathrm{d}z. \tag{9}$$

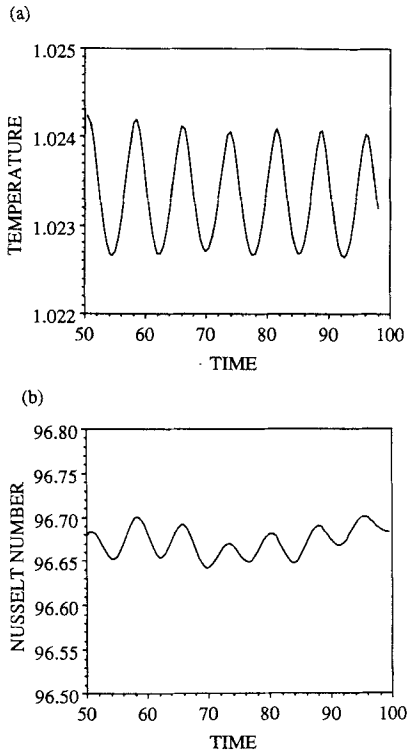

Figure 3. Time histories of the local temperature and the overall Nusselt number ($Ra=10^{10}$): (a) temperature at $(x, y, z)=(0{\cdot}510, 0{\cdot}810, 0{\cdot}517)$; (b) overall Nusselt number at the cooled wall at $x=0$

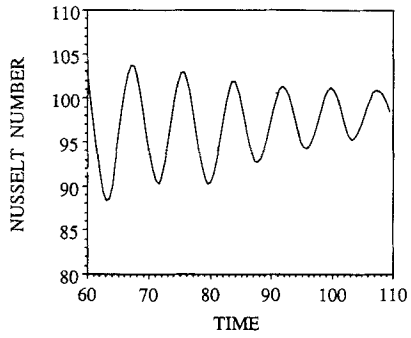

Figure 4. Evolution of the overall Nusselt number at the midplane $z=0{\cdot}5$ of the enclosure at $Ra=10^{10}$

Figure 5 shows the changes in the overall Nusselt number at the isothermal walls. The time-averaged Nusselt number is considered at $Ra=10^{10}$. For comparison purposes the same figure includes the two-dimensional predictions[2,3,18] and the three-dimensional numerical results[11] that are available in the literature. A logarithmic relationship is plotted in the figure. In the relatively low-Rayleigh-number flow regime ($Ra \leqslant 10^8$) the present three-dimensional data agree reasonably well with the two-dimensional computations. In this regard the two-dimensional heat

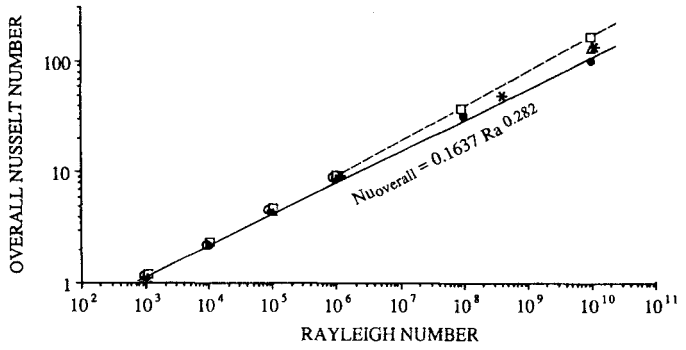

Figure 5. Changes in the overall Nusselt number with the Rayleigh number: ——, present 3D computations; – – –, Markatos and Pericleous;[2] ●, present 3D computations; □, Markatos and Pericleous[2] (2D); ○, de Vahl Davis[3] (2D); △, Silva and Emery[18] (2D); *, Lankhorst and Hoogendoorn[11] (3D)

transfer rate appears to be a good first estimate for the case of the realistic cubical enclosure with thermally insulated endwalls ($z=0$ and 1).

In contrast, considerable discrepancies are present among the predictions in the high-Rayleigh-number flow regime (e.g. at $Ra=10^{10}$). Substantial differences are discernible between the overall Nusselt numbers calculated by the present three-dimensional results and the previous two-dimensional predictions.[2,18] Various causes may be thought of, such as the difference in turbulence models adopted in the prior computations and the number of grid points, among others. However, at this juncture no conclusive statements could be made in the light of the lack of reliable experimental measurements and the insufficient data of full-scale three-dimensional computations.

Utilizing the above numerical results, the following expression for the heat transfer correlation over $10^3 \leqslant Ra \leqslant 10^{10}$ for the three-dimensional enclosure is proposed:

$$Nu_{\text{overall}} = 0{\cdot}163\, Ra^{0{\cdot}282}. \tag{10}$$

It is recalled that Markatos and Pericleous[2] determined the correlations over the Rayleigh number range $10^3 \leqslant Ra \leqslant 10^{16}$ for the two-dimensional air-filled enclosure as

$$Nu_{\text{overall}} = 0{\cdot}143\, Ra^{0{\cdot}299} \quad (10^3 \leqslant Ra \leqslant 10^6), \tag{11}$$

$$Nu_{\text{overall}} = 0{\cdot}082\, Ra^{0{\cdot}329} \quad (10^6 \leqslant Ra \leqslant 10^{12}). \tag{12}$$

As mentioned above, the differences in the heat transfer rates between the two- and three-dimensional results are appreciable as the Rayleigh number increases.

CONCLUSIONS

In the present numerical study an extensive series of high-resolution three-dimensional unsteady flow analyses has been performed on natural convection in a differentially heated cubical enclosure. The detailed structures of the fields were scrutinized by advanced numerical visualizations techniques. Over the studied range of Rayleigh number $10^3 \leqslant Ra \leqslant 10^{10}$, three-dimensional variations in the fields and the heat transfer rate were found to be confined to the regions near the endwalls as the Rayleigh number increased. Both the similarities and discrepancies between the present three-dimensional and preceding two-dimensional predictions are pointed out. These

underscore the significance of the three-dimensional computations in evaluating high-Rayleigh-number flows and the associated heat transfer properties.

APPENDIX: NOMENCLATURE

c_p	specific heat at constant pressure
Fr	Froude number, u_0^2/g^*L_0
g	gravitational acceleration
k	thermal conductivity
L_0	reference length (enclosure height)
N	Brunt–Väisälä frequency, $[g^*\beta^*(T_H-T_C)/L_0]^{1/2}$
p	pressure
p_0	reference pressure (hydrostatic pressure)
Pr	molecular Prandtl number, $c_p^*\mu^*/k^*$
Ra	Rayleigh number, $g^*\beta^*c_p^*\rho^{*2}L_0^3(T_H-T_C)/\mu^*k^*$
Re	Reynolds number, $\rho^*u_0L_0/\mu^*$
t	time
T	temperature
T_0	reference temperature, $(T_C+T_H)/2$
T_C, T_H	cooled and heated sidewall temperatures
u_0	reference velocity, $[g^*\beta^*L_0(T_H-T_C)]^{1/2}$
u, v, w	velocity components in the x-, y- and z-directions
x, y, z	Cartesian co-ordinates

Greek symbols

β	thermal expansion coefficient
δ	overheat ratio, $(T_H-T_C)/T_0$
μ	viscosity
ρ	density

Superscript

*	dimensional quantities

REFERENCES

1. S. Ostrach, 'Natural convection heat transfer in cavities and cells', *Proc. 7th Int. Heat Transfer Conf., Vol. 1*, Hemisphere Publishing, Washington, DC, 1978, pp. 365–379.
2. N. C. Markatos and K. A. Pericleous, 'Laminar and turbulent natural convection in an enclosed cavity', *Int. J. Heat Mass Transfer*, **27**, 755–772 (1984).
3. G. de Vahl Davis, 'Natural convection of air in a square cavity: a bench mark numerical solution', *Int. j. numer. methods fluids*, **3**, 249–264 (1983).
4. S. Paolucci and D. R. Chenoweth, 'Transition to chaos in a differentially heated vertical cavity', *J. Fluid Mech.*, **201**, 379–410 (1989).
5. J. Patterson and J. Imberger, 'Unsteady natural convection in a rectangular cavity', *J. Fluid Mech.*, **100**, 65–86 (1980).
6. G. N. Ivey, 'Experiments on transient natural convection in a cavity', *J. Fluid Mech.*, **144**, 389–401 (1984).
7. S. M. Han, 'A transient numerical analysis of high Rayleigh number convection in a differentially heated square cavity', *ASME Paper 84-HT-57*, 1984.
8. S. W. Armfield, 'Direct simulation of unsteady natural convection in a cavity', *Proc. Int. Symp. on Computational Fluid Dynamics*, Japan Soc. Fluid Mech., Tokyo, 1989, pp. 305–310.
9. G. D. Mallinson and G. de Vahl Davis, 'Three-dimensional natural convection in a box: a numerical study', *J. Fluid Mech.*, **83**, 1–31 (1977).

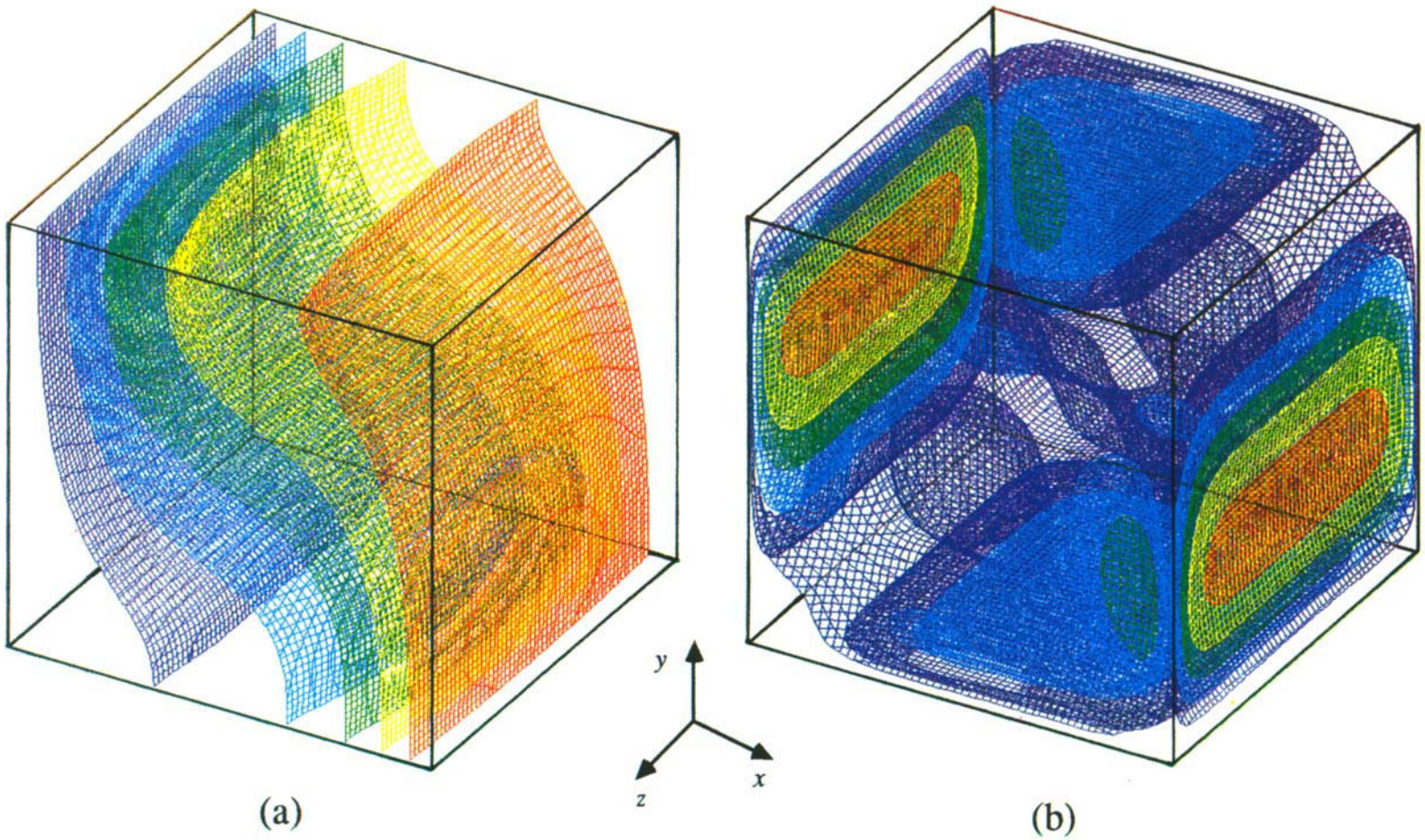

Plate 1. Surfaces of (a) the isotemperature and (b) the isovorticity (absolute values) at $Ra = 10^4$. Contour levels: (a) 0·9667 (purple), 0·9833 (blue), 1·0 (green), 1·017 (yellow), 1·033 (red); (b) 0·9 (purple), 1·8 (blue), 2·7 (green), 3·6 (yellow), 4·5 (red)

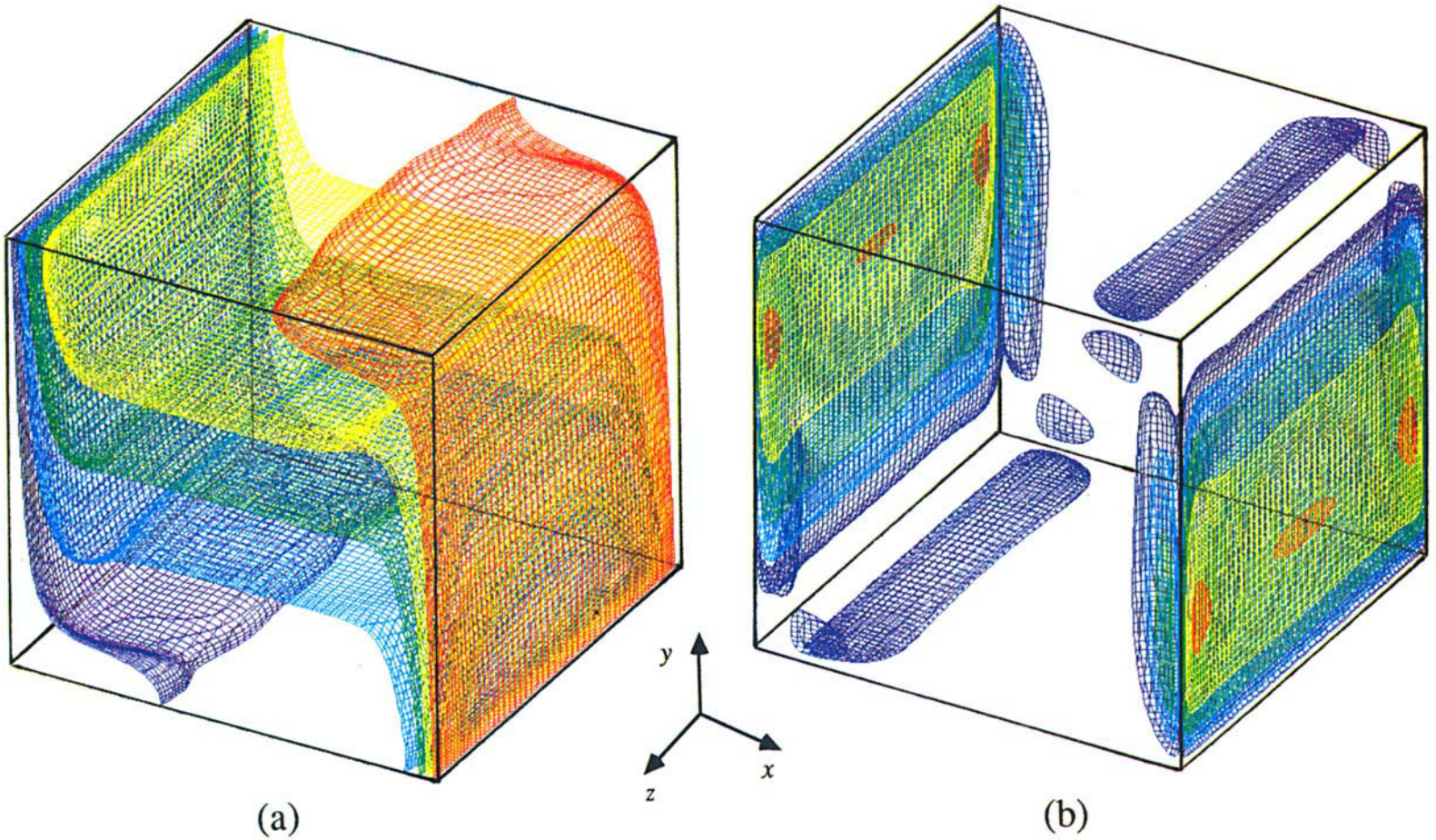

Plate 2. Surfaces of (a) the isotemperature and (b) the isovorticity (absolute values) at $Ra = 10^6$. Contour levels: (a) 0·9667 (purple), 0·9833 (blue), 1·0 (green), 1·017 (yellow), 1·033 (red); (b) 3·6 (purple), 7·2 (blue), 10·8 (green), 14·4 (yellow), 18·0 (red)

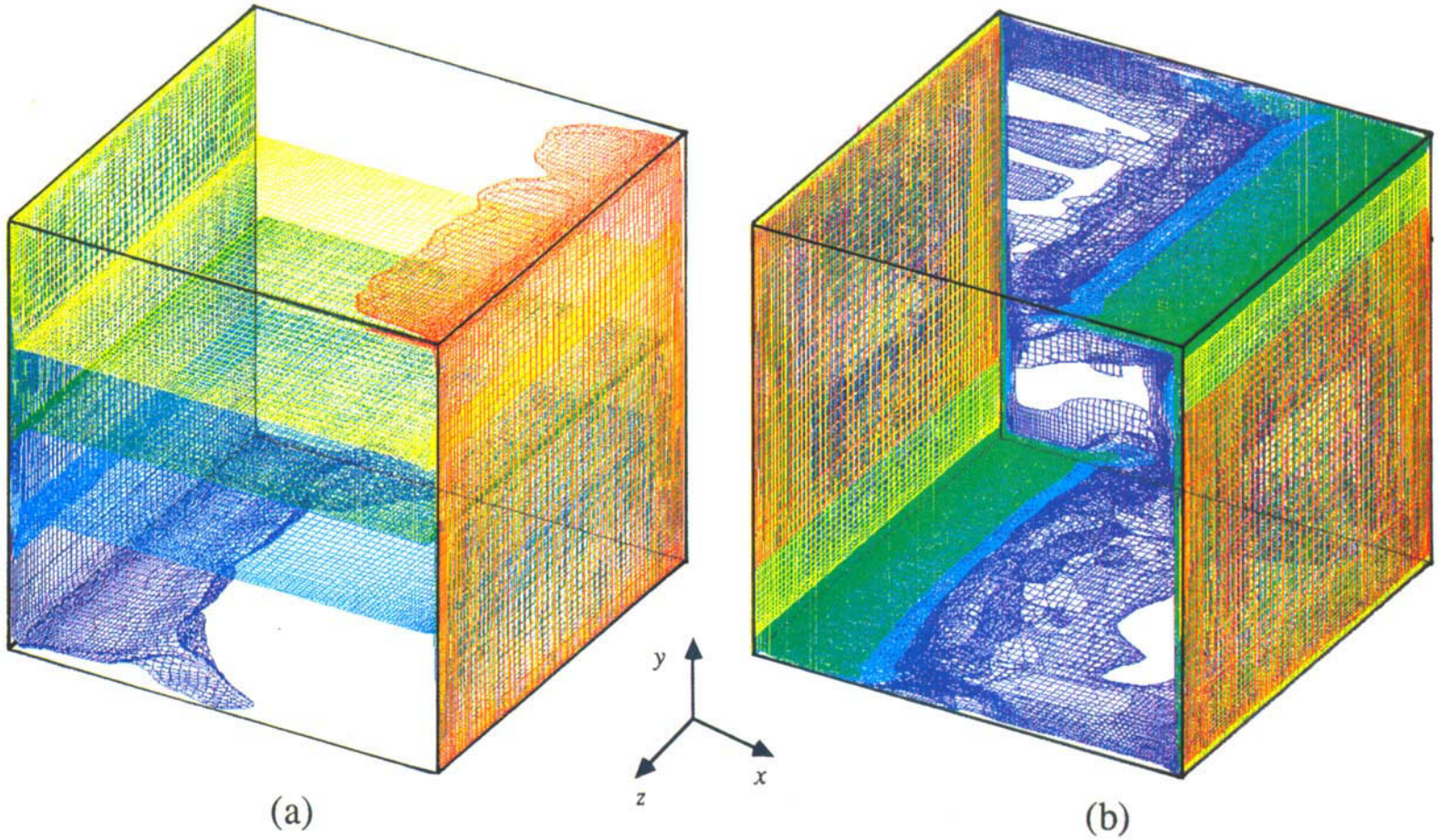

Plate 3. Surfaces of (a) the time-averaged isotemperature and (b) the time-averaged isovorticity (absolute values) at $Ra = 10^{10}$. Contour levels: (a) 0·9667 (purple), 0·9833 (blue), 1·0 (green), 1·017 (yellow), 1·033 (red); (b) 1·0 (purple), 5·0 (blue), 10·0 (green), 50·0 (yellow), 100·0 (red)

10. T. S. Lee, G. H. Son and J. S. Lee, 'Numerical predictions of three-dimensional natural convection in a box', *Proc. 1st KSME–JSME Thermal and Fluids Engineering Conf., Vol. 2*, KSME, Seoul, 1988, pp. 278–283.
11. A. M. Lankhorst and C. J. Hoogendoorn, 'Three-dimensional numerical calculations of high Rayleigh number natural convective flows in enclosed cavities', *Proc. 1988 Natl Heat Transfer Conf., Vol. 3*, ASME, New York, 1988, pp. 463–470.
12. S. V. Patankar, *Numerical Heat Transfer and Fluid Flow*, Hemisphere, Washington, DC, 1980.
13. H. L. Stone, 'Iterative solution of implicit approximations of multi-dimensional partial differential equations', *J. Numer. Anal.*, **5**, 530–558 (1968).
14. C. J. Freitas, R. L. Street, A. N. Findikakis and J. R. Koseff, 'Numerical simulation of three-dimensional flow in a cavity', *Int. j. numer. methods fluids*, **5**, 561–575 (1985).
15. S. Shirayama and K. Kuwahara, 'Patterns of three-dimensional boundary layer separation', *AIAA Paper 87-0461, 25th Aerospace Sciences Meeting*, 1987.
16. T. Fusegi, J. M. Hyun, K. Kuwahara and B. Farouk, 'A numerical study of 3-D natural convection in a differentially heated cubical enclosure', in *Simulation and Numerical Methods in Heat Transfer, ASME HTD Vol. 157*, ASME, New York, 1990, pp. 49–54.
17. J. M. Hyun and J. W. Lee, 'Numerical solutions for transient natural convection in a square cavity with different sidewall temperatures', *Int. J. Heat Fluid Flow*, **10**, 146–151 (1989).
18. D. J. Silva and A. F. Emery, 'A preliminary comparison of the k–ε and algebraic stress models for turbulent heat transfer in a square enclosure', in *Numerical Heat Transfer With Personal Computers and Supercomputing, ASME HTD Vol. 110*, ASME, New York, 1989, pp. 193–200.